Latent Characteristics and Neural Manifold of Brain Functional Network Under Acupuncture

Kai Li, Jiang Wang, *Member, IEEE*, Shanshan Li, Bin Deng, *Senior Member, IEEE*, and Haitao Yu

***Abstract*— Acupuncture can regulate the cognition of brain system, and different manipulations are the keys of realizing the curative effect of acupuncture on human body. Therefore, it is crucial to distinguish and monitor the different acupuncture manipulations automatically. In this brief, in order to enhance the robustness of electroencephalogram (EEG) detection against noise and interference, we propose an acupuncture manipulation detecting framework based on supervised ISOMAP and recurrent neural network (RNN). Primarily, the low-dimensional embedding neural manifold of brain dynamical functional network is extracted via the reconstructed geodetic distance. It is found that there exhibits stronger acupuncture-specific reconfiguration of brain network. Besides, we show that the distance travel along this manifold correlates strongly with changes of acupuncture manipulations. The low-dimensional brain topological structure of all subjects shows crescent-like feature when acupuncturing at Zusanli acupoints, and fixed-points are varying under diverse manipulation methods. Moreover, Takagi-Sugeno-Kang (TSK) classifier is adopted to identify acupuncture manipulations according to the nonlinear characteristics of neural manifolds. Compared with different classifier, TSK can further improve the accuracy of manipulation identification at 96.71%. The results demonstrate the effectiveness of our model in detecting the acupuncture manipulations, which may provide neural biomarkers for acupuncture physicians.**

***Index Terms*— Acupuncture, EEG, RNN, neural manifold.**

I. Introduction

ACUPUNCTURE is an essential treatment of traditional Chinese medicine, and its efficacy on various diseases has been confirmed by long-term clinical practice all over the world [1]–[3]. In the theory of traditional Chinese medicine, the basic role of acupuncture is to modulate the brain system, which plays an important role in the treatment of insomnia, stroke, and Alzheimer's disease [4], [5]. Apart from the functional treatment, acupuncture has multi-factor intervention, such as different manipulation methods: consists of twirling-rotating (TR) and lifting-thrusting (LT) of the needle. These methods can improve the stimulating effect of acupuncture on acupoints during the treatment procedure of acupuncture [6], [7]. Kim *et al.* [8] find that formalin-induced pain is significantly reduced in acupunctured by TR group and acupunctured by LT methods group, while TR is more effective than LT method. Furthermore, different acupuncture produces various influences on the blood perfusion with reinforcing LT or TR manipulation [9]. However, due to the complexity of physical operation, it is hard to monitor the acupuncture manipulations during the treatment procedure, and the acupuncture manipulations now mainly depend on physician's experience. There are few scientific evidences for the therapeutic effects of acupuncture manipulations. If the acupuncture manipulations cannot be quantified, the detailed effects of acupuncture manipulations are hard to be elucidated, which becomes an important shackle for the investigation of the treatment effect of acupuncture [10]. Therefore, it is urgent to develop an automatic acupuncture manipulations detection system, which can provide real-time manipulations detection.

In previous works, the acupuncture manipulations have been widely quantified via statistical table analysis or tactile detection [11], [12]. On this basis, in order to clarify the time-efficiency of acupuncture on brain activity, some researchers use nontraumatic brain imaging techniques for acupuncture decoding. In recent years, EEG is applied to investigate effects of acupuncture by recording neurophysiological signals in different brain regions [13]. Using nonlinear and multivariate statistics, Qi *et al.* [14] finds that acupuncture can activate brain regions except for the occipital lobes from EEG view. Yi *et al.* [15] finds that acupuncture may control and regulate information routing among brain regions from synchronous functional network. Due to high time-frequency characteristics of EEG, the signal can be used to detect the brain features in real time. However, Because of the existence of environmental noise, the robustness of decoding efficiency is affected. In this

Manuscript received November 11, 2021; revised December 30, 2021 and February 9, 2022; accepted February 27, 2022. Date of publication March 10, 2022; date of current version March 28, 2022. This work was supported in part by the National Natural Science Foundation of China under Grant 62071324, in part by the Natural Science Foundation of Tianjin under Grant 19JCYBJC18800, and in part by the Tianjin Research Innovation Project for Postgraduate Students under Grant 2021YJSB188. *(Corresponding author: Haitao Yu.)*

This work involved human subjects or animals in its research. Approval of all ethical and experimental procedures and protocols was granted by the Ethics Committee of Tangshan Gongren Hospital in China and performed in line with the Declaration of Helsinki.

The authors are with the School of Electrical and Information Engineering, Tianjin University, Tianjin 300072, China (e-mail: htyu@tju.edu.cn).

Digital Object Identifier 10.1109/TNSRE.2022.3157380

case, it is urgent to adopt a new EEG method to infer the latent states of brain circuits, which can detect the acupuncture manipulations more precisely. In this manner, we will abstract the brain as a dynamical functional network, and describe features of brain activity from low dimension view.

A significant limitation which has prevented the ubiquitous application of acupuncture detection is the morphological variability of the EEG signal. This makes it difficult to consistently extract the time-varying features of brain network [16]. At present, manifold learning allows us to extract latent neural states in the complex human brain activities, which is the key to realize the distinction and quantification of acupuncture [17]–[20]. Specifically, manifold is the sub-region which captures behavior in each task [21], [22]. Recent advances in neuroscience have demonstrated that neural manifold is present across brain regions, which provides idea for decoding brain activity [23]. Aoi *et al.* [24] finds that the rotation time-features of relevant task variables can be decoded according to the manifold geometry. Giszter *et al.* [25] finds that the desired behavior can be achieved by controlling a small number of independent latent factors. In this manner, the time-varying characteristics and stability of a single experiment can be analyzed from low-dimensional manifold. Therefore, from the perspective of manifold, it is possible to investigate the latent features of brain network and realize the quantification of acupuncture manipulations against noise and interference.

Recent advances in neuroscience have demonstrated that it is possible to study neural population activity using dimension reduction technique [26], [27]. Some dimensionality reduction techniques are used to find the low-dimensional manifold, such as principal component analysis (PCA) and multi-dimensional Scaling (MDS) [28]–[30]. Besides, nonlinear methods are used for learning manifolds with nonlinear characteristic, such as local linear mapping (LLE) and Isometric Feature Mapping (ISOMAP) [31], [32]. However, LLE requires that the manifold should not be closed. The method is sensitive to the value of the nearest neighbor sample number, and the sample set should be dense [33]. ISOMAP fails to make full use of fault sample information due to the unsupervised feature extraction way [34]. To obtain an accurate estimate of displacement along the manifold, the improved ISOMAP is used in this paper. Furthermore, recurrent neural network (RNN) is established to build a refactoring network [35], [36]. The historical features of low-dimensional manifolds are fed into RNN and are used to predict the current manifold features. Based on the actual and predicted manifolds geometry, the distance travelled by the signal along the manifold may be used to infer changes of latent brain characteristics under acupuncture, which can draw the differences between acupuncture manipulations more precisely.

By extracting neural manifold, we can decode latent information from complex EEG signals and quantify features which is more significant, especially with the development of machine learning method [37]. However, traditional learning methods cannot catch the accurate results when the system is with complex nonlinear features. Nevertheless, Takagi-Sugeno-Kang (TSK) classifier has performance interpretability in multiple features classification task [38], [39]. The advantage of such method is that the interpretability and accuracy of judgment can be synchronously taken [40]. In this manner, with the historical and predicted manifold features, the application of TSK can better explain the nonlinear features of brain system, and obtain a better quantification of acupuncture characteristics. Based on the manifold learning and TSK classification methods, we can extract the low-dimensional feature of EEG signals, which can improve the detection accuracy of manipulations.

II. Mathematical Model and Methods

A. Datasets

Acupuncture is an important treatment method in Traditional Chinese Medicine (TCM), which inserts needle into patient's acupoints at a certain angle. The acupuncture applied on the patient is located at 'Zusanli' (ST36, right side) acupoint, which is at the outside of the lower leg, three inches below the knee joint [41]. This experiment is raised by Tangshan Gongren Hospital, and some experiments are conducted in First Teaching Hospital of Tianjin University of Traditional Chinese Medicine. The experiment is conducted in accordance with the Declaration of Helsinki.

In this acupuncture experiment, the needles are performed by a professional acupuncturist. 25 healthy volunteers aged from 20 to 25 (13 females and 12 males), who have no prior knowledge of acupuncture and are not clear about the sequences, are involved in this study. Before the experiment, the test environment is set to be clean, comfortable, and quiet. Other ratio waves (such as mobile phones) are turned off during the experiment. The operating equipment should be disinfected before use. In the experiment, the healthy subjects are sitting in a quiet room for 5 minutes, keeping awake with their eyes closed. Subsequently, the doctor begins by rubbing the skin on acupoints, and push the needle into the skin with a depth of 2-3 mm. The subjects will feel acid during the stimulation procedure. In addition, a kind of acupuncture manipulation (LT or TR methods with a rotation frequency) is used at "Zusanli" acupoints for 2 minutes. Under the action of TR method, the right twist is mainly used and the silver needle is rotated from left to right. LT method is mainly needle lifting, slowly entering and quickly exiting the needle (Fig. 1).

For EEG signal, we choose 2 minutes in order to attain a more obvious stimulation effect. All EEG recordings are collected by an EEG amplifier from the 19 Ag-AgCl scalp electrodes for each subject. Placement is achieved by using an international standard 10-20 system. To eliminate the power line interference, all EEG recordings are first filtered from 0.5Hz to 50Hz by a band-passed finite impulse digital filter during preprocessing. Then the mean value of all channel signals is calculated as the reference potential. Ocular artifacts and muscle shaking are eliminated via independent component analysis (ICA). The time domain EEG signal is converted to frequency domain signal by fast Fourier transform:

$$\mathrm{Z(k)}=\sum_{n=1}^{N} z(n)e^{-j(\frac{2\pi}{N})nk} \tag{1}$$

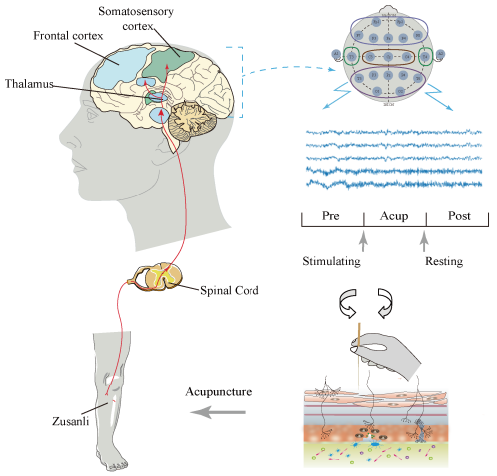

Fig. 1. Schematic diagram of acupuncture. Electroencephalographic signals evoked by manual acupuncture at "Zusanli" acupoint of healthy human subjects are directly recorded. The manipulations include TR and LT methods.

where Z(k) denotes the Fourier transformation of kth sample point. Furthermore, the frequency domain signal is filtered by rectangular window, and converted back to the time domain signal through inverse fast Fourier transform, such as:

$$z(n) = \frac{1}{N}\sum_{k=1}^{N} Z(k)e^{j(\frac{2\pi}{N})nk} \tag{2}$$

B. Graph Theory Analysis

Phase lag index (PLI) is applied to describe the phase synchronization between two signals in different brain regions ($Z(t)$). The PLI is obtained by calculating the asymmetry of instantaneous signal phase difference distribution between two brain regions, which reflects the degree of synchronous oscillation between the signal pairs. PLI is calculated as:

$$PLI = |\langle sign[\Delta\phi(Z(t_k))]\rangle|, \quad k = 1, 2, \ldots\ldots, N \tag{3}$$

where $\Delta\phi$ is the phase difference at time point t_k between two signals $Z(t_k)$. The value of PLI ranges from 0 to 1. 0 values indicates that there is no coupling between two timeseries. By calculating PLI for all time points in each epoch in all channels, we can obtain the strength of synchronization connection among brain regions. Based on the PLI adjacency matrix, dynamical functional brain networks (M) are reconstructed by setting a threshold. For graph theory parameters analysis, the clustering coefficient C_i of node i is defined as:

$$C = \frac{1}{N}\sum_{i=1}^{N} 2E_i/[k_i(k_i-1)] \tag{4}$$

where E_i is the actual number of edges between neighboring nodes of node i, and N is the number of nodes within network. Global efficiency can be defined as:

$$E_{global} = \frac{1}{N(N-1)}\sum_{i,j,i\neq j}^{N}\frac{1}{d_{ij}} \tag{5}$$

Local efficiency of network is the average of local efficiency of all nodes, which can be calculated to measure the segregation property of network. It is shown as:

$$E_{lobal}(k) = \frac{1}{NN_{G_k}(N_{G_k}-1)}\sum_{k=1}^{N}\sum_{i,j,i\neq j}^{N}\frac{1}{d_{ij}} \tag{6}$$

Small world network (SWN) index can be defined as:

$$S = \frac{E_{global}}{E_{rand}}\cdot\frac{C}{C_{rand}} \tag{7}$$

The SWN index is calculated by an average of 1000 random network implementations. Compared with random network, SWN is more sensitive to information routing among nodes.

C. Neural Manifold Estimation

The method of manifold extraction is improved Isometric Feature Mapping (I-ISOMAP). The low-dimensional eigen structures of high-dimensional data centers are calculated via global manifold feature extraction. In this manuscript, the above brain dynamical functional network vectors (M) are taken as input space and mapped to adjacent points by means of graph theory (Fig. 2). All columns in the lower triangle of dynamic functional network (M) are concatenated as a correlation vector (H), which represents the time-dependent connection of dynamic functional network. Furthermore, the vectors (H) are composed into a manifold G in the input space X, and the manifold of EEG is calculated. First of all, the average value of each feature in acupuncture manipulation category is taken as the center vector (l). The relationship between the eigenvalue j of i-th sample point ($z_{i,j}$) and the eigenvalue sample point of center vector is $sim_j(i,k)$, such as:

$$sim_j(i,k) = \frac{\sqrt{\left|z_{i,j}^2 - l_{k,j}^2\right|}}{2} \tag{8}$$

Meanwhile, the fuzzy entropy is used to describe the fuzzy degree of acupuncture sample points to categories. We assume that there are m features, the sum of fuzzy entropy of all features of sample point X to class I is defined as:

$$\begin{aligned} H(x,i) = -\sum_{j=1}^{m}[&sim_j(i,k)\times\ln(sim_j(i,k)) \\ &+(1-sim_j(i,k))\times\ln(1-sim_j(i,k))] \end{aligned} \tag{9}$$

We take the membership degree of sample point X to class i as:

$$L(z,i) = e^{-H(z,i)} \tag{10}$$

The more likely the sample points are belonging to this class when the degree of membership is greater. In addition, the sample reliability is calculated to infer the degree of characterization of data from different sample points:

$$K(z) = -\sum_{k=1}^{c} L(z,i)\ln(L(z,i)) \tag{11}$$

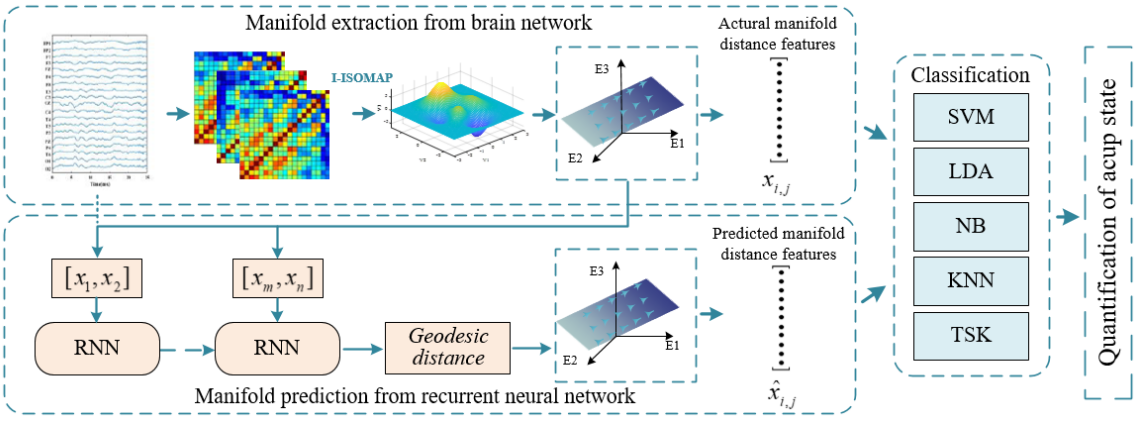

Fig. 2. The framework for extraction of neural manifold and classification of acupuncture states. EEG is coded in the functional network, and is sent to the ISOMAP method to extract the manifold geometry features and distance features. Besides, the historical manifold features are sent to RNN to get the current manifold features. Both actual and predicted manifold are fed into classification for the quantification of acupuncture states.

Furthermore, the geodesic distance matrix is defined as:

$$D(x_i, x_j) = \begin{cases} \sqrt{1 - \exp(-\sqrt{K_i K_j} d(z_i, z_j)/\beta)}, & y_i = y_j \\ \sqrt{\exp(\sqrt{K_i K_j} d(z_i, z_j)/\beta) - \alpha}, & y_i \neq y_j \end{cases} \tag{12}$$

$$\beta = \frac{\sum d(z_i, z_j)}{N} \quad i, j = 1, 2, \ldots, N \tag{13}$$

K is the sample reliability, $d(z_i, z_j)$ is the Euclidean distance between sample data z_i and z_j. y is the category label of z. β is used to prevent $D(z_i, z_j)$ from growing too fast with $d(z_i, z_j)$. α is used to control the distance between samples.

Furthermore, Floyd algorithm is adopted to measure the shortest path. Classical MDS algorithm is used to construct the embedded coordinate representation of data in D-dimensional space Y, and any two embedded coordinate vectors y_i and y_j are selected to minimize the cost function:

$$\min \quad \phi(Y) = \sum_{i=1}^{N} \sum_{j=1}^{N} (D_{ij}^{G} - \|y_i - y_j\|)^2 \tag{14}$$

Meanwhile, plane coefficient is used to measure the geometry features of neural manifold (m, o, p). Using the least squares method, we set the correlation among network nodes as $p = a_1 m + a_2 o + a_3$, and calculate the relative plane degree:

$$S = \sum (p_{ij} - \widehat{p}_{ij})^2 / S_{mean}. \tag{15}$$

Besides, the node clustering coefficient (4) is used to measure the low-dimensional manifold clustering features. The distances of nodes: $R = \sqrt{(m_1 - m_2)^2 + (o_1 - o_2)^2 + (p_1 - p_2)^2}/2$, and the relative radius is measured as the norm approximate of largest distances between nodes.

In this manner, I-ISOMAP is built on the basis of MDS and retains the essential geometric structure of nonlinear data, namely the geodesic distance between point pairs. Because the vector represents the changes of dynamic functional network over time, the mapped low-dimensional manifold can indicate the intrinsic characteristics of different brain regions under acupuncture stimulation. From low-dimensional analysis, we can extract the main neural characteristics which is related to acupuncture manipulations. Therefore, we can raise the robustness of detection against noise and interference, which can be used to detect the acupuncture manipulations precisely.

D. Manifold Feature Prediction Based on RNN

In order to get more accurate quantification, we use the manifold (G) at historical moment to predict the manifold feature (x_t) of current moment via RNN. The architecture is:

$$f_t = \sigma(W_f[h_{t-1}, x_t] + b_f) \tag{16}$$

$$\dot{i}_t = \sigma(W_i[h_{t-1}, x_t] + b_i) \tag{17}$$

$$\tilde{C}_t = \tanh(W_c[h_{t-1}, x_t] + b_c) \tag{18}$$

$$C_t = \sigma(f_t \times C_{i-1} + i_t \times \tilde{C}_t) \tag{19}$$

$$o_t = \sigma(W_i[h_{t-1}, x_i] + b_o) \tag{20}$$

$$h_t = o_t \times \tanh(C_t) \tag{21}$$

where W represents the weight matrix of each gate, and b represents the bias. Finally, the hidden state h_t is the final output. For training, the historical manifold features are fed into RNN as input, and the current manifold features are taken as output. Under testing procedure, the current features will be predicted by the historical manifold sequences. Differences of acupuncture manipulations will be detected by comparing the features of actual neural manifolds and constructed manifolds. The differences between testing and prediction are evaluated by mean absolute percentage error (MAPE):

$$MAPE = \frac{1}{n} \sum_{i=1}^{n} \frac{|h_t - h_{real}|}{h_{real}} \tag{22}$$

E. Takagi-Sugeno-Kang (TSK) Fuzzy Model

Given manifold G input dataset $\mathbf{X} = \{\mathbf{x}_1, \mathbf{x}_2, \ldots, \mathbf{x}_n\} \in \mathbf{R}^d$ and the corresponding class label set $\mathbf{Y} = \{y_1, y_2, \ldots, y_n\}$, where $y_i, i = 1, 2, \ldots, N$ represent the corresponding class,

the k th fuzzy inference rules are often defined as

$$R^k: \text{ IF } x_1 \text{ is } A_1^k \wedge x_2 \text{ is} A_2^k \wedge \ldots \wedge x_d \text{ is} A_d^k,$$
$$\text{THEN} f_k(\mathbf{x}) = \beta_0^k + \beta_1^k x_1 + \ldots + \beta_d^k x_d, \quad k = 1, \ldots, K$$

where $\mathbf{x} = [x_1, x_2, \ldots, x_d]^T$ is input vector of each rule, K is the number of fuzzy rules, A_i^k are Gaussian antecedent fuzzy sets subscribed by the input variable x_i of Rule k, $\wedge$ is a fuzzy conjunction operator, $f_k(\mathbf{x})$ is a linear function of the inputs, and β_i^k are linear parameters. With each rule is premised on the sample vector $\mathbf{x}$ the output of a TSK fuzzy system can be expressed as:

$$\tilde{y} = \sum_{k=1}^{K} \frac{\mu_k(\mathbf{x}) f_k(\mathbf{x})}{\sum_{k'=1}^{K} \mu_{k'}(\mathbf{x})} = \sum_{k=1}^{K} \tilde{\mu}_k(\mathbf{x}) f_k(\mathbf{x}) \tag{23}$$

where

$$\mu_k(\mathbf{x}) = \prod_{i=1}^{d} \mu_{A_i^k}(x_i) \tag{24}$$

$$\tilde{\mu}_k(\mathbf{x}) = \mu_k(\mathbf{x}) / \sum\nolimits_{k'=1}^{K} \mu_{k'}(\mathbf{x}) \tag{25}$$

are the fuzzy membership function and the normalized fuzzy membership function of the antecedent parameters of the kth fuzzy rule. While $\mu_{A_i^k}(x_i)$ is Gaussian membership function for fuzzy set A_i^k that can be expressed as

$$\mu_{A_i^k}(x_i) = \exp\left(-\left(x_i - c_i^k\right)^2 / \delta_i^k\right) \tag{26}$$

where c_i^k is kth cluster center parameters that is obtained by the classical fuzzy c-means (FCM) clustering algorithm:

$$c_i^k = \sum_{j=1}^{N} u_{jk} x_{ji} / \sum_{j=1}^{N} u_{jk} \tag{27}$$

and the width parameter δ_i^k can be estimated by

$$\delta_i^k = h \cdot \sum_{j=1}^{N} u_{jk} \left(x_{ji} - c_i^k\right)^2 / \sum_{j=1}^{N} u_{jk} \tag{28}$$

where the element $u_{jk} \in [0, 1]$ denotes the fuzzy membership of the n-th input sample $\mathbf{x}_n$ to the k th cluster ($k = 1, 2, \ldots, K$), h is a constant called the scale parameter.

For an input sample $\mathbf{x}_n$, let

$$\begin{aligned}
\mathbf{x}_{n,e} &= \left(1, \mathbf{x}_n^T\right)^T \\
\tilde{\mathbf{x}}_n^k &= \tilde{\mu}^k(\mathbf{x}_n)\, \mathbf{x}_e \\
\rho(\mathbf{x}_n) &= \left(\left(\tilde{\mathbf{x}}_n^1\right)^T, \left(\tilde{\mathbf{x}}_n^2\right)^T, \ldots, \left(\tilde{\mathbf{x}}_n^K\right)^T\right)^T \in R^{K(d+1)} \\
\boldsymbol{\beta}^k &= \left(\beta_0^k, \beta_1^k, \ldots, \beta_d^k\right)^T \\
\boldsymbol{\beta}_g &= \left(\left(\boldsymbol{\beta}^1\right)^T, \left(\boldsymbol{\beta}^2\right)^T, \ldots, \left(\boldsymbol{\beta}^K\right)^T\right)^T
\end{aligned} \tag{29}$$

then the output value $\tilde{y}_n$ of a TSK fuzzy classifier is:

$$\tilde{y}_n = \boldsymbol{\beta}_g^T \rho(\mathbf{x}_n) \tag{30}$$

III. Numerical Results

A. Analysis of Brain Functional Controllability

Primarily, the controllability of brain network under different acupuncture manipulations during cognitive process is investigated via dynamical functional network analysis. The controllability is referred as integration and separation of brain functional network. Dynamic functional network can reflect the process of dynamic information transmission among different brain regions over a period, which reflects the controllability of acupuncture. In this paper, the sliding window method is adopted, and each time window is regarded as a Time Point (TP) in the dynamical network.

Based on dynamical functional network (DFN), we extract network features such as time clustering coefficient (C), local efficiency (L), global efficiency (G) and small world index (SWI) to analyze the controllability of DFN under different acupuncture stimulation and time windows. Primarily, the effect of time window is investigated. In order to choose the appropriate window length, the sliding window length of 0.5s, 1s, 2s, 3s, 4s, 6s and 10s are selected respectively to analyze the fluctuation of brain dynamical synchronous network. The size of windows ensures that the EEG signals with the length of 2 min would not cause fragment loss when applying the sliding window. Rank-sum statistical test is used to investigate the influence of different window lengths on the stability of brain time-varying features under different manipulations.

Under the same time scale, the clustering coefficient and local efficiency of TR is higher than that of LT and resting states, which indicates that the average clustering effect of all brain network nodes increase under the manipulation of TR methods. Meanwhile, the global efficiency and small world index of TR is higher, which shows good integration of brain regions and good ability of information transmission when manipulating TR method. Furthermore, time-varying features of network controllability is conducted via dynamical complex network analysis. High value of global efficiency indicates high controllability of TR method, which shows that acupuncture has more control effect in the neural information transmission of brain network. It indicates that brain functional controllability increases with the TR method. Meanwhile, the functional controllability of LT method is higher than resting state, which shows that acupuncture can modulate the functional integration and controllability, while TR method is better than that of LT method. Besides, we can draw the conclusion that acupuncture can modulation the controllability of brain states, and different manipulations have various effect.

Moreover, it is shown that the neural interactions between different brain regions of all subjects are less affected by time when the time length is short. With the increase of time length, the clustering coefficient tends to be stable after 3s. It is found that the differences of time clustering coefficient and local efficiency among subjects gradually decreases with the increase of time scale. Especially, with the increase of time scale, the global efficiency and small world index among groups show a trend of increasing, and the maximum value appears at the time length of 3s. Besides, the temporal attribute of network is gradually manifested, and the ability of local functional

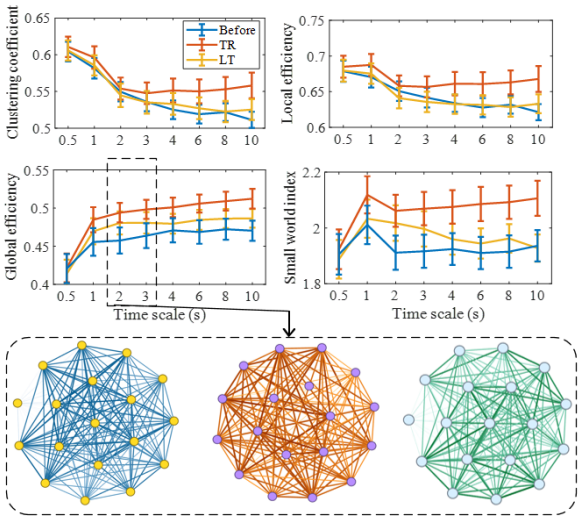

Fig. 3. The dynamical neural network analysis according to the different brain states of acupuncture: before acupuncture (BA), TR and LT. The blue curve, red curve and yellow curve represent the information of subjects in the resting state (before acupuncture), TR state and LT state, respectively.

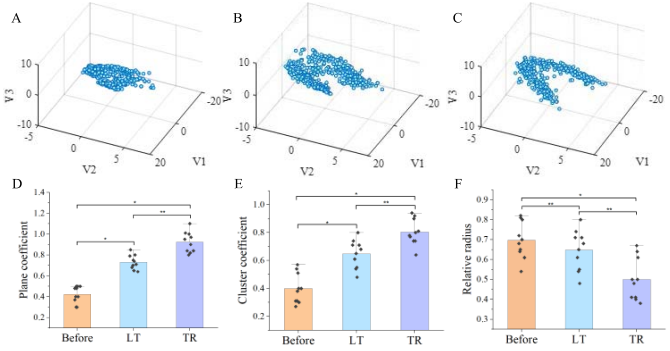

Fig. 4. Analysis of cerebral neural manifold under acupuncture. (4A-4C): From left to right, the three-dimensional topological structure of resting state, LT state, and TR state. Fig. 4D is the flatness degree of the three-dimensional manifold; Fig. 4E is the three-dimensional manifold clustering coefficient; Fig. 4F shows the relative radius of the two-dimensional manifold.

integration of brain changes over time. These results indicate that the dynamic functional network of brain is affected by time length, and provide support for the latent controllability analysis of different acupuncture stimulation manipulations. Therefore, the time scale for dynamical functional network will be chosen at 3s in the latent manifold analysis.

B. Analysis of Brain Manifold Topology Under Different Acupuncture Manipulations

Based on the controllability analysis of dynamical functional network, the low-dimensional manifold structural features of different acupuncture states (including resting, LT and TR state) are extracted to distinguish the latent neural features of different acupuncture effects (Fig. 4).

Primarily, the planar diagram of three-dimensional manifold structure of resting state is taken from the dynamical functional network (Fig. 4A). The distribution of dynamical functional structure is relatively concentrated without fixed shape. The manifold state under LT and TR acupuncture methods is extracted. Compared with resting state, the three-dimensional topology manifold of brain under acupuncture tends to be a single plane, while the network forms a regular crescent structure. Under LT method, the three-dimensional topology of manifold connection is more divergent, and the central bulge of plane forms a peak-like shape, which is in obvious contrast with the resting state topology before acupuncture (Fig. 4B). Under TR method, the three-dimensional topology of manifold connection is more compact. The structure of shortest distance between topological points is more prominent and the shape of crescent is more appropriate (Fig. 4C).

To be more specific, the dynamical manifold structure is quantified by clustering coefficient and plane degree among resting, LT and TR states. Primarily, the plane coefficient is obtained (Fig. 4D). Using the least squares methods, we calculate the flat flatness error as the relative plane degree of neural manifold under acupuncture. It is found that the manifold plane degree of human brain in resting state is low. On the contrast, the plane degree of brain in LT and TR state increases, and the plane of TR manifold is more consistent. However, the plane degree of manifold structure under LT methods is less flat than that of TR methods, but it is flatter than the resting manifold structure. The node clustering coefficient is used to calculate the low-dimensional manifold clustering features (Fig. 4E). It is found that the relative clustering coefficient of neural manifold structure in the resting state is 0.4, which is lower than that of LT and TR states. In addition, changes in relative radius of three-dimensional manifolds under different states are shown in Fig. 4F, which is consistent with the results reflected by the manifold clustering coefficient.

These results indicate that acupuncture at ‘Zusanli’ acupoints has the ability to regulate brain function and improve the dynamic behavioral characteristics of brain. The three-dimensional manifold structure under acupuncture is more concentrated, which is coherent with the controllability analysis of brain network. From the perspective of low-dimensional manifolds, it can be found that the effects of different acupuncture have obvious differences: the neural manifolds under TR method are more concentrated, and the clustering coefficient of manifolds is larger. Under LT method, the mapping plane of low-dimensional manifolds is sparse, the clustering coefficient of manifolds is small, but the curvature radius of manifolds is large. It is shown that three-dimensional manifold plane structure of brain is more compact under TR manipulation, which shows TR has better regulation effect. Besides, by combining sample reliability and sample label information, the improved ISOMAP algorithm redefines the geodesic distance matrix of traditional ISOMAP method. To illustrate the effectiveness of the proposed algorithms, the low-dimensional manifold structures under different dimension-reduction methods are calculated, and the average interclass separability parameter are taken as evaluation criterion. The results are shown in Table I.

It is shown that the proposed method improves the traditional ISOMAP methods: the intra-class distance gets reduced

TABLE I
INTERCLASS SEPARABILITY OF EACH MANIFOLD-EXTRACTION METHOD

Method	Separability	Method	Separability
PCA	0.0412	ISOMAP	0.0871
LLE	0.0915	I-ISOMAP	0.1154

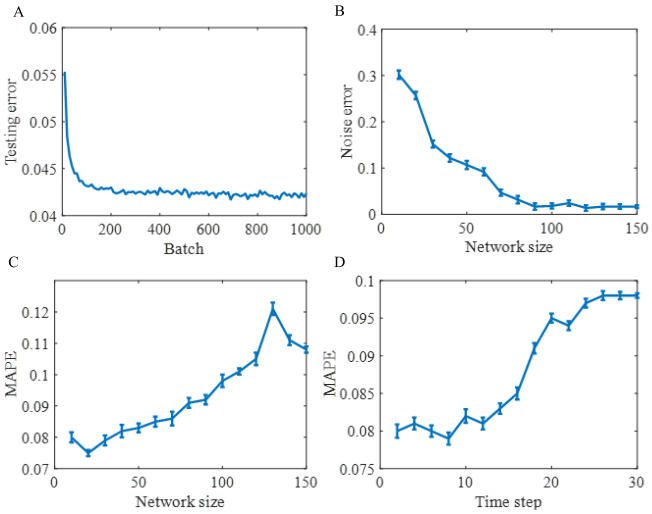

Fig. 5. Effect of manifold prediction by RNN. Fig. 5A: Testing error with the training batches; Fig. 5B: Noise error with the network size; Fig. 5C: MAPE with the network size; Fig. 5D: MAPE with the time step.

and the inter-class distance gets increased by considering the reliability of samples and labels of different acupuncture manipulations. Therefore, the neural manifold under various acupuncture manipulations can be better adopted.

Furthermore, the manifold prediction is evaluated by RNN (Fig. 5). The testing error is calculated with the evolution of training bathes. With the increase of training batches, the testing error decreases dramatically and becomes stable when the batch is over 400 (Fig. 5A). In addition, the robustness of RNN when predicting the current manifold is evaluated (Fig. 5B). It is shown that the noise error decreases with the enhancement of network size, which indicates that the number of hidden neurons can affect the learning ability of model network. This result is proved by MAPE in Fig. 5C. MAPE increases with the network size, and the peak is achieved when the network size is 130. It means that the testing effect is best when the network size is 130 and it would get worse when the network size increases continually. As for the batch size of data input, it controls the frequency of updating weight. In order to analyze the influence of input batch size on model prediction accuracy, the time step of input is set from 0-30. The MAPE increases with the enhancement of timestep without obvious changes, which means that the time step of input sequences will not affect the precision of prediction.

C. Analysis of Brain Time-Varying Features Based on Neural Manifold Under Different Acupuncture Frequencies

The neural time-varying features of different acupuncture methods can be distinguished by low-dimensional manifold. Furthermore, the dynamical evolution process of manifold under different acupuncture frequencies (50, 100, and 150 times/min) are investigated. Apart from the intrinsic neural manifold, the distance travelled along the manifold can be used to infer the time-varying changes of brain network under acupuncture manipulations. The change effect of three-dimensional manifold of brain under TR method are shown in Fig 6A-6C. As can be seen from Fig. 6A, in the process of acupuncture, the neural manifold of human brain presents a crescent shape, and the changes of brain dynamical functional network evolve along the time-frequency trajectory of neural manifold from the end to the middle, reflecting the rotary tuning features of acupuncture.

With the continuous increase of acupuncture frequency, the relative rotation radius of manifold structure increases. It is shown that the relative rotation radius of three-dimensional manifold structure is the largest when the acupuncture frequency is 150 times per minute. With the increase of stimulus frequency, the structural density of three-dimensional neural manifold will decrease. Meanwhile, the planar structure characteristics of brain dynamic manifolds under stimulation frequencies are shown in Fig 6D-6F. Under different acupuncture stimulation frequencies, convergence points appear in the central region of three-dimensional manifold structure. With the decrease of stimulation frequency, the planar structure of manifold becomes more concentrated when the stimulation frequency is 50 times per minute, while the planar structure of neural manifold becomes more discrete when the stimulation frequency is 150 times per minute. It is found that the TR manipulation at 'Zusanli' acupoint has a significant effect of modulating functional activities of brain when the stimulation frequency is at 50 times per minute. It can be explained by the fast response speed of brain time-varying points along neural manifold.

Besides, the manifold characteristics of LT method under different stimulation frequencies are shown in Fig 6G-6I. It is shown that the neural manifold structure of brain is crescent under LT method, and the rotational radius of neural manifold increases with the enhancement of stimulation frequency from geometry view. Especially, the rotational radius of neural manifold is the largest when the acupuncture frequency is 150 times per minute. Under the effect of same stimulation frequency, the rotation radius of neural manifold structure of brain under the action of LT is larger than that of TR method, while the radius of manifold structure and relative density are lower. These results indicate that the dynamical functional network structure of brain is relatively sparse under LT method. The plane of manifold structure under LT method is shown in Fig. 6J-6L, and it is found that there are two convergence points in the center of manifold structure under LT method. In this manner, the faster response speed of dynamical functional trajectory and better effect of acupuncture will be achieved when the frequency of acupuncture stimulation is smaller.

More specifically, the shortest distance statistics of neural manifold structure under TR method are shown in Fig. 7A. The shortest distance indicates the evolution process of the dynamical functional network during acupuncture procedure.

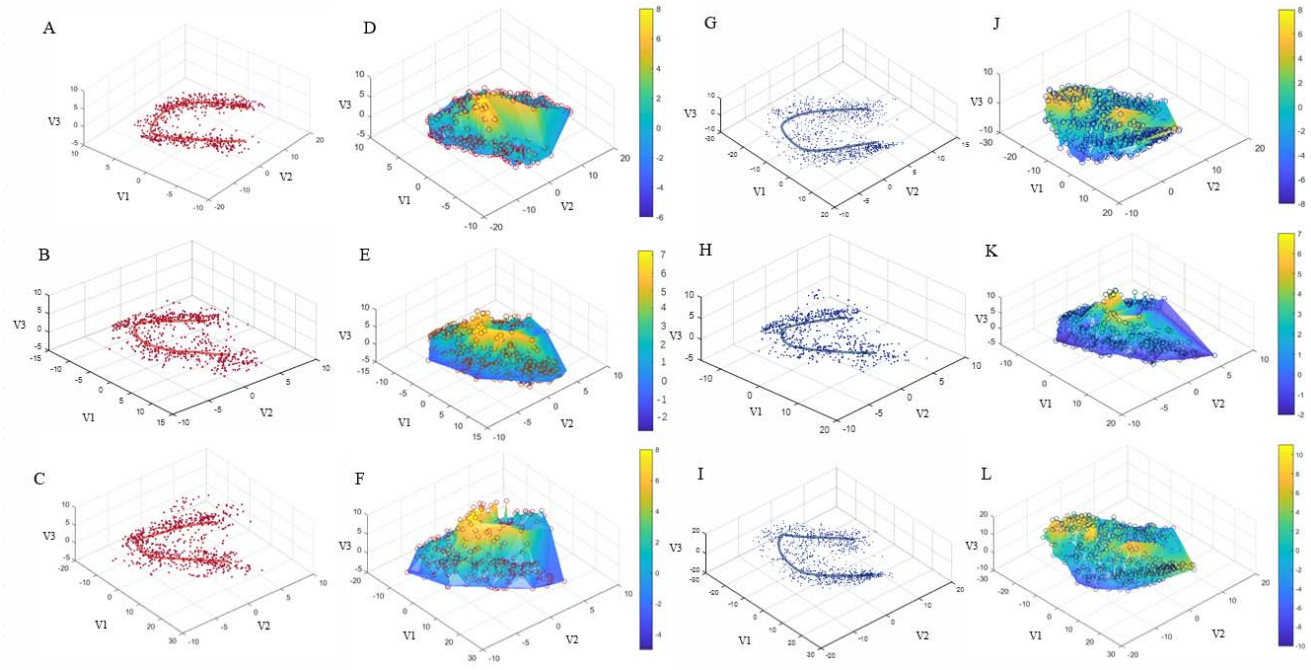

Fig. 6. Analysis of neural manifold structure of brain under different acupuncture manipulations and different acupuncture frequencies. From left to right, and from top to bottom, the brain three-dimensional manifold topology analysis is performed under the action of acupuncture frequency of 50, 100 and 150 times per minute, respectively, in the state of acupuncture TR and LT.

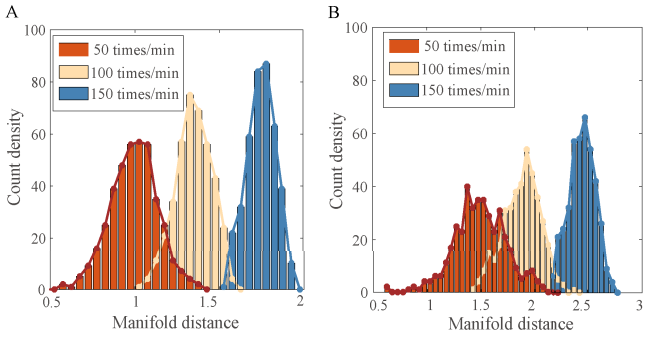

Fig. 7. Statistical analysis of the euclidian distance between adjacent points in the neural manifold of brain under different acupuncture manipulations and different acupuncture frequencies. (7A) TR method (7B) LT method.

With the shortest distance between nodes decreases, the evolution speed of functional network increases. It is found that the shortest distance of manifold is smaller when the stimulation frequency is smaller under TR method. The manifold distance from the center point is about 1, which shows the characteristic of normal distribution. Neural manifold distance increases with the enhancement of stimulation frequency. Count density is also growing meanwhile, which suggests that the distribution of neural manifolds will get more spread out when the acupuncture stimulation frequency is larger.

Compared with TR method, the statistics of shortest distance of three-dimensional neural manifold structure of brain under LT method is shown in Fig. 7B. Under corresponding stimulus frequencies, the manifold distance between adjacent points of three-dimensional manifold increases when the LT method is applied. Similarly, with the enhancement of stimulus frequency, the count of larger manifold distance points increases. However, compared with TR method, the rotation density of neural manifold decreases with the same of stimulus frequency under LT method. Particularly, when the frequency of acupuncture stimulation is 50 times per minute, the shortest distance between the points of three-dimensional neural manifold is the smallest, and the neural manifold is relatively concentrated. It is shown that the shortest distance between points of LT manifold is larger and neural manifold is more dispersed under the same stimulation frequency.

Furthermore, the latent time-varying characteristics along two-dimensional manifold under different stimulation frequencies are analyzed based on the original manifold characteristics. The trajectory characteristics of two-dimensional neural manifold changes in brain under TR method is shown in Fig. 8. The two-dimensional manifold topology of brain under TR method presents a regular crescent shape and fluctuates around the only fixed point in the centre. With the implementation of different manipulations, the brain time-varying features under acupuncture stimulation moves different crescent directions towards fixed point along the manifold.

To determine the differences of brain time-varying features under acupuncture manipulations, we begin by visualizing the trends in the manifold. Gradation in neural manifold along the X-axis of resulting manifold can indicate the latent factors of the manifold and brain time-varying features under acupuncture can be estimated with manifold mapping. In Fig 8A, it can be conducted the neural manifold is dense at the middle, while it shows sparse in the two ends of manifold. We set the middle point of neural manifold as fixed point. With the increase of acupuncture frequency, the radius of

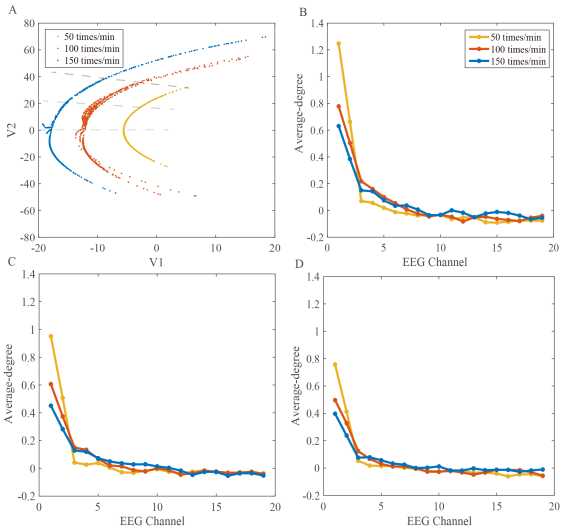

Fig. 8. Time-varying characteristics along manifolds under TR manipulation. Fig. 8A shows the manifold corresponding to different acupuncture frequencies; Fig. 8B-8D represent the average degree of functional network corresponding to the manifold near and far from the stability point, respectively.

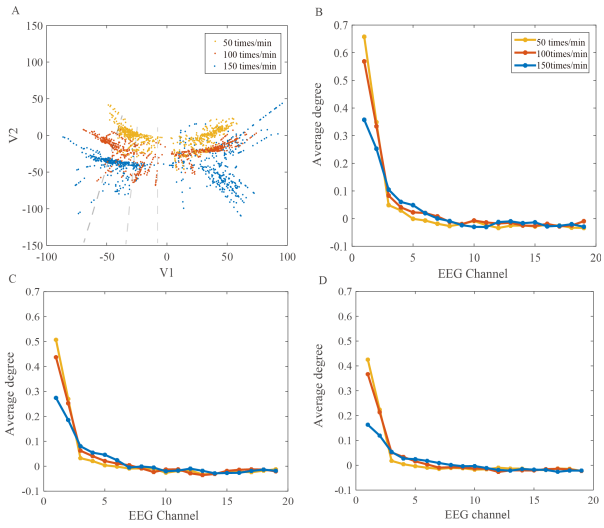

Fig. 9. Time-varying characteristics of manifolds under LT manipulation. Fig. 9A shows the manifolds corresponding to acupuncture frequencies. Fig. 9B-9D represent the characteristics values of functional network corresponding to the manifold near and far from the stability point, respectively.

manifold structure becomes larger. When the frequency of acupuncture reaches 150 times per minute, the radius of neural manifold has reached the maximum, which indicates that neural manifold is aggregated at fixed point in the crescent shape under TR method. Meanwhile, with the enhancement of acupuncture frequency, the distance between the fixed point and other points along the manifold increases, while the state of fixed point will migrate. The radius of two-dimensional manifold increases, indicating that the evolution speed of two-dimensional manifold trajectory of brain is different under stimulation frequencies. However, when the stimulation frequency is 50 times per minute, the acupuncture effect can be realized quickly and the stability is strong. Therefore, the modulation effect of brain system is better when stimulation frequency is low under TR method.

For the time-evolution features along the manifold, the variation of scatted features of manifold near the fixed point is investigated (Fig. 8B- Fig. 8D). At each manifold point, the average degree of each channel is calculated, which represents the interaction features of network. It shows that the degree of functional network corresponding to the frontal region of brain is larger, while the degree of other brain regions is smaller. It indicates that brain regions involved in the acupuncture is mainly the frontal region, and the acupuncture is related to tactile and conscious perception. Meanwhile, it is found that the average degree of dynamical functional network corresponding to the same manifold point decreases with the increase of stimulation frequency (Fig. 8B), which means that acupuncture has the best effect when the stimulation frequency of acupuncture is 50 times per minute. The trajectory far from the fixed point is investigated. It is found that the characteristic values of dynamical functional network near the stability point are relatively high, while decreases with the increasing distance between selected parameter points and stability point (Fig. 8C-8D). It is shown that the time-varying features of acupuncture stimulation manifold reaches fixed point from original point, and then gradually fluctuates along the direction of inward diffusion of the fixed point. The trajectory shown by low-dimensional trajectory of manifold is consistent with the structure of manifold. This result is also related to the gradual migration of fixed point of manifold with the increase of stimulus frequency.

Manifold time-varying features under LT method are investigated with different acupuncture frequencies. The trajectory along the neural manifold under LT method is obviously clustered into two parts, and the two-part manifold time-varying features fluctuates around the two fixed points (Fig. 9A). For LT methods, brain dynamic under acupuncture stimulation switches between two fixed points, indicating that brain dynamically forms two neural state characteristics under LT method. With the increase of stimulation frequency, the radius of neural manifold expands and the degree of dispersion of manifold aggregation points increases. Two-dimensional manifold scatted points with different distances from the fixed point are selected on one side.

The average degrees of dynamical functional network near the fixed point of trajectory are reflected (Fig. 9B). It is found that the average degrees of frontal lobe are larger, which shows that acupuncture effects on brain areas mainly at the frontal area, while it is associated with tactile awareness and consciousness. Meanwhile, with the increase of stimulation frequency, the average degrees of manifolds corresponding to dynamical functional network points gradually decreases, which has the same effect as the TR method. Compared with Fig. 9C-9D, the average degree of dynamical functional network corresponding to the manifold points near stability point are relatively high, while the average degree of functional network corresponding to the manifold points decrease with the increase of stability distance. The results show that neural activities are gradually diffused outward from the fixed point

TABLE II
CLASSIFICATION RESULTS BASED ON DIFFERENT MANIFOLD FEATURES

Input parameter	accuracy	sensitivity	specificity	Original data
d_{actual}	0.8412	0.8579	0.8252	0.7133
$d_{predicted}$	0.8324	0.8217	0.8342	0.7085
$d_{actual}+d_{predicted}$	**0.9671**	**0.9214**	**0.9519**	**0.7722**

TABLE III
CLASSIFICATION RESULTS BASED ON DIFFERENT CLASSIFIER METHODS

Input parameter	accuracy	sensitivity	specificity	Original data
SVM	0.8257	0.8719	0.9012	0.6418
LDA	0.8642	0.8145	0.8208	0.6329
KNN	0.9154	0.8977	0.9052	0.6251
NB	0.9218	0.9119	0.8948	0.6697
TSK	**0.9671**	**0.9214**	**0.9519**	**0.7722**

along the manifold structure, and the structure forms a fixed point-half crescent shape. From the manifold geometry and time-varying features view, it can be concluded that the acupuncture manipulations of LT are quite different from that of TR methods, and the distance along the neural manifold can be used to distinguish and monitor the variation of acupuncture stimulation frequencies.

D. Quantification of Acupuncture EEG Manifold

Based on the geometry and time-varying features of neural manifold analysis, the manifold features extracted by I-ISOMAP and RNN are used as the input of TSK quantification. The training set (including data collection and label set) is randomly divided into 10 subsets. In that case, one feature and combined feature are chosen in TSK training. The optimal input vector and classification results are shown in Table II. It can be concluded that for the actual manifold feature, adding the predicted manifold feature as common inputs can improve the classification results. With the combination of actual and predicted feature, the accuracy, sensitivity, and specificity get increased dramatically, which is better than taking single manifold signal as input. In this way, it is crucial to choose an appropriate input features combination via machine learning.

Meanwhile, for the original EEG data, the accuracy achieves 77.22% when taking actual and RNN predicted signals as TSK inputs. It is found that the combination of actual and RNN predicted signal can take better accuracy results when compared with single signals. Moreover, the accuracy can be enhanced with the use of manifold characteristics. Under the combination of manifold and RNN predicted signals, the accuracy can be reached at 96.71%. In addition, TSK algorithm is compared with the other four traditional Linear methods commonly used in machine identification, including SVM, Linear Discriminant Analysis (LDA), Naive Bayesian (NB) and K-Nearest Neighbor (KNN) algorithm. The combined manifold features are selected as input for various classifiers simultaneously, and the recognition results are in Table III.

It can be observed from the table that for manifold features, linear classifier in the NB method is the optimal classification, and identification accuracy can reach 92.18%. Besides, the TSK classifier can show better classification effect than the linear classifier. The decoding of neural manifold is better than that of original EEG signals. To test the processing pipeline in the presence of noise, we build the synthetic datasets (while noise signal is added, and the effective mean value of the noise signal is between $0 \sim 0.2$ times of origin EEG signal). The acupuncture manipulation method proposed perform better than original decoding methods mentioned in the presence of noise, and the ground truth for the signal is verified. Our result is a comprehensive analysis of the intrinsic manifold of brain while stimulated by acupuncture, which can be applied for the decoding of manifold and the design of acupuncture BCI.

IV. CONCLUSION AND DISCUSSIONS

In this paper, in order to enhance the robustness of EEG detection against noise and interference, we propose an acupuncture manipulation detection method based on the combination of I-ISOMAP and RNN. Primarily, the features of brain dynamical functional network are investigated under acupuncture manipulations. It is found that brain network shows high integration function and controllability under TR method. In addition, the low-dimensional manifold of brain functional network under different acupuncture manipulations is extracted based on the model. From the geometry view, low dimensional structure of manifold under acupuncture shows crescent-shaped characteristics, and the radius enlarges with the increase of acupuncture frequencies. It is found that the trajectory along neural manifold under LT method is obviously clustered into two parts, while the trajectory under TR method is from end to middle along neural manifold. Based on the manifold features, TSK can further improve the quantification accuracy of acupuncture manipulation at 96.71%. These results indicate the robustness of this model in detecting the acupuncture manipulation automatically, which may provide a novel neural biomarker for acupuncture physicians.

For network controllability analysis, investigation of the control properties of complex networks can provide insights into how they can be promoted to achieve desired behaviors [42]. Cai *et al* [43] use functional controllability to investigate the dynamic causal brain circuits during working memory. Scheid *et al* [44] investigate the controllability of effective connectivity network during seizure progression for the determination of optimal personalized stimulation parameters. In the paper, the trajectory of brain functional network under acupuncture are used to measure the controllability of

acupuncture. Higher global efficiency reflects better network controllability, which means lower average control energy needed to drive networks from a given set of nodes. In this work, we find that the differences of clustering coefficient and local efficiency among the groups of subjects gradually decreases with the increase of time scale. For the same time scale, the clustering coefficient and local efficiency of TR is higher than that of LT and normal states, which shows that the average clustering effect of all nodes increases with the manipulation of TR method. Besides, the global efficiency and small world index among groups increase with the time scale. This result emphasizes the cognitive context-dependent controllability under acupuncture, which may provide new insight into how acupuncture works with brain circuit.

Furthermore, the analysis of neural manifolds has consistently uncovered the latent features of brain network, which captures a significant fraction of neural variability [20], [45], [46]. It is indicated that, although the relationship between activity pattern and acupuncture content changes over time, the representational geometry could remain relatively constant. In this work, we define the theoretical framework based on the combination of I-ISOMAP and RNN to investigate the low-dimensional manifold during acupuncture task. Compared with original ISOMAP method, we improve the original model by introducing the concept of sample reliability, and the geodesic distance matrix is redefined by combing the sample reliability and the sample category label. The intra-class distances are reduced, while the inter-class distances are increased and the sample separability is accelerated. With the combination of actual and RNN-predicted manifold features, the manifold features of different acupuncture manipulations can get better distinguished. Among structural characteristics of low-dimensional manifold, there is one fixed point in TR manifold, while two fixed point in LT manifold. It indicates that TR manipulation has features of convergence and stability, which makes brain network more concentrated. The LT method has divergent effect and poor stability, where brain latent geometry is more discrete, reflecting the characteristics of acupuncture controllability techniques. These results can have further implications which transcend acupuncture manipulation estimated by EEG signals. In other words, the observation of consistent low-dimensional manifold structure in in EEG signal suggest that the brain activity has low intrinsic dimensionality despite their appearance in high-dimensional space. Therefore, the geometry and time-varying features along manifold can be used to motor and quantify the modulation effect of acupuncture on brain against noise and interference.

In this paper, the decoding model combining manifold dimensionality reduction approaches with machine learning is designed. With the reduction of model parameters, it can be easier to improve the decoding efficiency of acupuncture manipulations. Compared with different classifier, TSK method has higher interpretability by integrating the advantages of nonlinear rules and membership functions [47]. Particularly, via extracting the intrinsic manifold of brain network under acupuncture stimulation, the robustness of the model against noise and interference gets raised. Consequently, our results provide a model framework to monitor the brain time-varying evolution procedure under acupuncture automatically. It will be of great significance to decode the brain characteristics under acupuncture stimulation, and provide neural biomarker of acupuncture manipulations. There are still some limitations in our research. The analysis of EEG depends on the sensor level, which restricts the interpretation of the findings. Future works may focus on designing more accurate algorithms to extract neural manifold with higher decoding accuracy.

REFERENCES

[1] M. S. Lee, B. C. Shin, and E. Ernst, "Acupuncture for Alzheimer's disease: A systematic review," *Int. J. Clin. Pract.*, vol. 63, no. 6, pp. 874–879, 2009.

[2] R. Manber, R. N. Schnyer, J. J. B. Allen, A. J. Rush, and C. M. Blasey, "Acupuncture: A promising treatment for depression during pregnancy," *J. Affect. Disorders*, vol. 83, no. 1, pp. 89–95, Nov. 2004.

[3] L. Zhao *et al.*, "The long-term effect of acupuncture for migraine prophylaxis: A randomized clinical trial," *JAMA Internal Med.*, vol. 177, no. 4, pp. 508–515, 2017.

[4] Y. Lu *et al.*, "Brain areas involved in the acupuncture treatment of AD model rats: A PET study," *BMC Complementary Alternative Med.*, vol. 14, no. 1, p. 178, Dec. 2014.

[5] J. Xiong *et al.*, "The effect of combined scalp acupuncture and cognitive training in patients with stroke on cognitive and motor functions," *NeuroRehabilitation*, vol. 46, no. 1, pp. 75–82, Feb. 2020.

[6] R. T. Davis, D. L. Churchill, G. J. Badger, J. Dunn, and H. M. Langevin, "A new method for quantifying the needling component of acupuncture treatments," *Acupuncture Med., J. Brit. Med. Acupuncture Soc.*, vol. 30, no. 2, pp. 113–119, 2012.

[7] M. Silvers, "Acupuncture wins BMA approval," *Brit. Med. J.*, vol. 321, no. 7252, p. 11, 2000.

[8] G. H. Kim, M. Yeom, C. S. Yin, H. Lee, I. Shim, and M. S. Hong, "Acupuncture manipulation enhances anti-nociceptive effect on formalin-induced pain in rats," *Neurolog. Res.*, vol. 32, no. 1, pp. 92–95, 2010.

[9] X. Li *et al.*, "The influence of skin microcirculation blood perfusion at Zusanli acupoint by stimulating with lift-thrust reinforcing and reducing acupuncture manipulation methods on healthy adults," *Evidence-Based Complementary Alternative Med.*, vol. 2013, pp. 1–7, Jan. 2013.

[10] S. Sangtin, T. Supasiri, R. Tangsathitporn, and K. Pongpirul, "Application of survival analysis techniques to determine the optimal number of acupuncture therapy sessions for stroke patients," *Acupuncture Med.*, vol. 38, no. 3, pp. 194–200, Jun. 2020.

[11] B. Chen, K. Lin, L. Xu, J. Cao, and S. Gao, "A piezoelectric force sensing and gesture monitoring-based technique for acupuncture quantification," *IEEE Sensors J.*, vol. 21, no. 23, pp. 26337–26344, Dec. 2021.

[12] Y. Shen *et al.*, "Electroacupuncture for lumbar disc herniation A protocol for systematic review and meta-analysis," *Medicine*, vol. 99, no. 17, pp. 1–6, 2020.

[13] H. Yu, X. Wu, L. Cai, B. Deng, and J. Wang, "Modulation of spectral power and functional connectivity in human brain by acupuncture stimulation," *IEEE Trans. Neural Syst. Rehabil. Eng.*, vol. 26, no. 5, pp. 977–986, May 2018.

[14] S.-Y. Qi *et al.*, "Using nonlinear dynamics and multivariate statistics to analyze EEG signals of insomniacs with the intervention of superficial acupuncture," *Evidence-Based Complementary Alternative Med.*, vol. 2020, pp. 1–13, Nov. 2020.

[15] G. Yi *et al.*, "Ordinal pattern based complexity analysis for EEG activity evoked by manual acupuncture in healthy subjects," *Int. J. Bifurcation Chaos*, vol. 24, no. 2, Feb. 2014, Art. no. 1450018.

[16] A. Taebi, B. E. Solar, A. J. Bomar, R. H. Sandler, and H. A. Mansy, "Recent advances in seismocardiography," *Vibration*, vol. 2, no. 1, pp. 64–86, 2019.

[17] R. B. Ebitz and B. Y. Hayden, "The population doctrine in cognitive neuroscience," *Neuron*, vol. 109, no. 19, pp. 3055–3068, Oct. 2021.

[18] R. Zhang, G. S. Kranz, and T. M. C. Lee, "Functional connectome from phase synchrony at resting state is a neural fingerprint," *Brain Connectivity*, vol. 9, no. 7, pp. 519–528, Sep. 2019.

[19] B. Feulner and C. Clopath, "Neural manifold under plasticity in a goal driven learning behaviour," *PLOS Comput. Biol.*, vol. 17, no. 2, Feb. 2021, Art. no. e1008621.

[20] J. A. Gallego, M. G. Perich, S. N. Naufel, C. Ethier, S. A. Solla, and L. E. Miller, "Cortical population activity within a preserved neural manifold underlies multiple motor behaviors," *Nature Commun.*, vol. 9, no. 1, p. 4233, Oct. 2018.

[21] J. A. Gallego, M. G. Perich, L. E. Miller, and S. A. Solla, "Neural manifolds for the control of movement," *Neuron*, vol. 94, no. 5, pp. 978–984, 2017.

[22] H. S. Seung and D. D. Lee, "The manifold ways of perception," *Science*, vol. 290, no. 5500, pp. 2268–2269, 2000.

[23] B. Feulner and C. Clopath, "Neural manifold under plasticity in a goal driven learning behaviour," *PLOS Comput. Biol.*, vol. 17, no. 2, Feb. 2021, Art. no. e1008621.

[24] M. C. Aoi, V. Mante, and J. W. Pillow, "Prefrontal cortex exhibits multidimensional dynamic encoding during decision-making," *Nature Neurosci.*, vol. 23, no. 11, pp. 1410–1420, Nov. 2020.

[25] S. F. Giszter, "Motor primitives—New data and future questions," *Current Opinion Neurobiol.*, vol. 33, pp. 156–165, Aug. 2015.

[26] A. D. Degenhart *et al.*, "Stabilization of a brain-computer interface via the alignment of low-dimensional spaces of neural activity," *Nature Biomed. Eng.*, vol. 4, no. 7, pp. 1–14, 2020.

[27] X. Li *et al.*, "Latent factor decoding of multi-channel EEG for emotion recognition through autoencoder-like neural networks," *Frontiers Neurosci.*, vol. 14, p. 87, Mar. 2020.

[28] L. Chen and A. Buja, "Local multidimensional scaling for nonlinear dimension reduction, graph drawing, and proximity analysis," *J. Amer. Statist. Assoc.*, vol. 104, no. 485, pp. 209–219, 2009.

[29] R. D. Flint *et al.*, "The representation of finger movement and force in human motor and premotor cortices," *Eneuro*, vol. 7, no. 4, Jul. 2020.

[30] Q. M. J. Lin *et al.*, "Cerebellar neurodynamic predict decision timing and outcome on the single-trial level," *Cell*, vol. 180, no. 3, pp. 536–551, 2020.

[31] R. Huang, G. Zhang, and J. Chen, "Semi-supervised discriminant isomap with application to visualization, image retrieval and classification," *Int. J. Mach. Learn. Cybern.*, vol. 10, no. 6, pp. 1269–1278, Jun. 2019.

[32] H. Li and M. Trocan, "Sparse reconstruction of ISOMAP representations," *J. Intell. Fuzzy Syst.*, vol. 37, no. 6, pp. 7519–7536, Dec. 2019.

[33] J. P. Cunningham and B. M. Yu, "Dimensionality reduction for large-scale neural recordings," *Nature Neurosci.*, vol. 17, no. 11, pp. 1500–1509, 2014.

[34] B. Ghojogh *et al.*, "Multidimensional scaling, sammon mapping, and I-ISOMAP: Tutorial and survey," 2020, *arXiv:2009.08136*.

[35] Z. Zhang, H. Cheng, and T. Yang, "A recurrent neural network framework for flexible and adaptive decision making based on sequence learning," *PLOS Comput. Biol.*, vol. 16, no. 11, Nov. 2020, Art. no. e1008342.

[36] Y. Fathi and A. Erfanian, "A probabilistic recurrent neural network for decoding hind limb kinematics from multi-segment recordings of the dorsal horn neurons," *J. Neural Eng.*, vol. 16, no. 3, Jun. 2019, Art. no. 036023.

[37] C. Men, J. Wang, B. Deng, X.-L. Wei, Y.-Q. Che, and C.-X. Han, "Decoding acupuncture electrical signals in spinal dorsal root ganglion," *Neurocomputing*, vol. 79, pp. 12–17, Mar. 2012.

[38] Y. Jiang *et al.*, "Seizure classification from EEG signals using transfer learning, semi-supervised learning and TSK fuzzy system," *IEEE Trans. Neural Syst. Rehabil. Eng.*, vol. 25, no. 12, pp. 2270–2284, Dec. 2017.

[39] Y. Zhang *et al.*, "Seizure classification from EEG signals using an online selective transfer TSK fuzzy classifier with joint distribution adaption and manifold regularization," *Frontiers Neurosci.*, vol. 14, pp. 2–8, Jun. 2020.

[40] Z. Cao, W. Ding, Y.-K. Wang, F. K. Hussain, A. Al-Jumaily, and C.-T. Lin, "Effects of repetitive SSVEPs on EEG complexity using multiscale inherent fuzzy entropy," *Neurocomputing*, vol. 389, pp. 198–206, May 2020.

[41] F. Lai *et al.*, "Acupuncture at Zusanli (ST36) for experimental sepsis: A systematic review," *Evidence-Based Complementary Alternative Med.*, vol. 2020, pp. 1–16, Mar. 2020.

[42] J. Ruths and D. Ruths, "Control profiles of complex networks," *Science*, vol. 343, no. 6177, pp. 1373–1376, Mar. 2014.

[43] W. Cai, S. Ryali, R. Pasumarthy, V. Talasila, and V. Menon, "Dynamic causal brain circuits during working memory and their functional controllability," *Nature Commun.*, vol. 12, no. 1, p. 3314, Dec. 2021.

[44] B. H. Scheid *et al.*, "Time-evolving controllability of effective connectivity networks during seizure progression," *Proc. Nat. Acad. Sci. USA*, vol. 118, no. 5, Feb. 2021, Art. no. e2006436118.

[45] A. Arieli, A. Sterkin, A. Grinvald, and A. Aertsen, "Dynamics of ongoing activity: Explanation of the large variability in evoked cortical responses," *Science*, vol. 273, pp. 1868–1871, Sep. 1996.

[46] H. Yu, X. Li, X. Lei, and J. Wang, "Modulation effect of acupuncture on functional brain networks and classification of its manipulation with EEG signals," *IEEE Trans. Neural Syst. Rehabil. Eng.*, vol. 27, no. 10, pp. 1973–1984, Oct. 2019.

[47] H. Yu, X. Lei, Z. Song, C. Liu, and J. Wang, "Supervised network-based fuzzy learning of EEG signals for Alzheimer's disease identification," *IEEE Trans. Fuzzy Syst.*, vol. 28, no. 1, pp. 60–71, Jan. 2020.